

Anisotropic light-shift and magic-polarization of the intercombination line of Dysprosium atoms in a far-detuned dipole trap

Thomas Chalopin,¹ Vasiliy Makhalov,¹ Chayma Bouazza,¹ Alexandre Evrard,¹ Adam Barker,² Jean Dalibard,¹ Raphael Lopes,^{1,*} and Sylvain Nascimbene¹

¹*Laboratoire Kastler Brossel, Collège de France, CNRS, ENS-PSL Research University, UPMC-Sorbonne Universités, 11 place Marcelin Berthelot, F-75005 Paris, France*

²*Clarendon Laboratory, University of Oxford, Oxford OX1 3PU, United Kingdom*

We characterize the anisotropic differential AC Stark shift for the Dy 626 nm narrow line transition, induced in a far-detuned 1070 nm optical dipole trap, and observe the existence of a “magic polarization” for which the polarizabilities of the ground and excited states are equal. From our measurements we extract both the scalar and tensorial components of the dynamic dipole polarizability for the excited state, $\alpha_e^s = 179(5) \alpha_0$ and $\alpha_e^t = 35(2) \alpha_0$, respectively, where α_0 is the atomic unit for the electric polarizability. Furthermore, we utilize our findings to optimize the efficiency of Doppler cooling of a trapped gas, by controlling the sign and magnitude of the inhomogeneous broadening of the optical transition.

Lanthanide atoms offer a new and exciting test bed on which to explore long-awaited physical phenomena such as the appearance of the roton-excitation in dipolar Bose-Einstein condensates, due to their large magnetic moments, [1–4] or the occurrence of exotic superfluid phases based on narrow transition lines and a dense Feshbach resonance spectrum [5–9].

These unique properties arise thanks to the partially-filled, submerged 4f shell but, due to the large number of unpaired electrons, come with a drawback in terms of complexity. For instance, the dynamic (dipole) polarizability, which is of fundamental importance as it sets the strength of light-matter interactions, is theoretically challenging to estimate [10–12]. Several experimental efforts have been made to benchmark these theoretical models but have, so far, only addressed the polarizability of the ground state [13–15].

In the case of the 626 nm (intercombination) narrow-line transition used in several dysprosium (Dy) cold atom experiments, little is known about the excited state polarizability [16–18]. Besides its fundamental interest, its characterization plays an important role when considering the action of near-resonant light on a gas confined in the high-intensity field of an optical dipole trap [19]. In particular, for different polarizabilities between ground and excited states, one expects a shift of the resonance line proportional to the trapping light intensity (differential light-shift).

For lanthanide atoms, due to the significant tensorial contribution to the total atomic polarizability, the differential light-shift strongly depends on the trapping light polarization [13, 15]. This offers the possibility to locally vary the transition resonance frequency by fine-tuning the trapping beam polarization; a feature that has also been applied in a similar manner to alkali atoms, using the differential vectorial polarizability [20]. Such a feature could be exploited, for instance, to detune a cooling laser beam from the denser region of a trapped atomic cloud [21] or to cancel the inhomogeneous transition broadening, an effect particularly interesting for op-

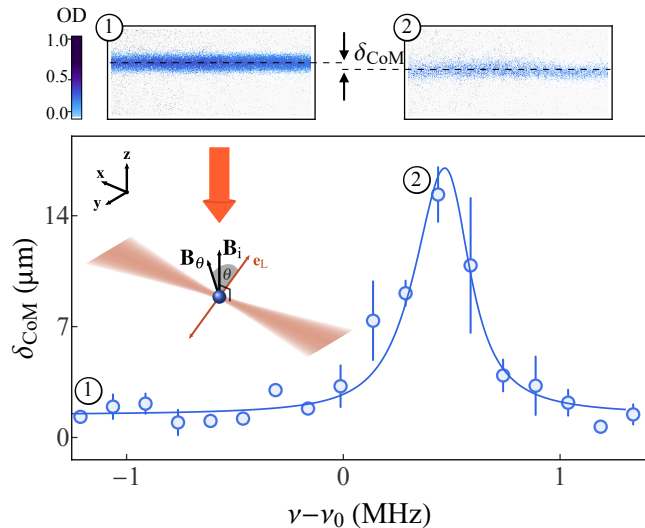


FIG. 1. Center-of-mass displacement resonance. Schematic drawing: a near-resonant (626 nm) red beam is applied to a cold atomic sample optically trapped around the focal point of a 1070 nm laser beam propagating along the x axis. The magnetic field bias is orientated in a plane perpendicular to the optical beam propagation axis, forming an angle θ with the polarization vector e_L . Two orientations of \mathbf{B} are represented: the initial vertical orientation (\mathbf{B}_i) and the value corresponding to the resonance curve shown in the main panel (\mathbf{B}_θ). After application of the red beam (see text) the atoms are accelerated, leading to a displacement of the cloud center-of-mass (CoM), measured after time-of-flight (ToF) represented by the dashed lines (see top panels). The center-of-mass displacement (δ_{CoM}) is plotted as a function of the laser frequency ν for $\theta = 80^\circ$ and fitted using Eq. (7) with the free parameter $\Delta\alpha(\theta)$. The error bars denote the r.m.s. deviation of 3 independent measurements.

tical lattice clocks [22–26] and single atom imaging in optical lattices [27].

In this Article we characterize the anisotropic differential light-shift in the case of the ^{164}Dy 626 nm narrow-line transition ($|g\rangle = |J=8, m_J=-8\rangle \rightarrow |e\rangle = |J'=9, m_{J'}=-9\rangle$) for a cold gas trapped in a far-detuned 1070 nm optical trap (see Fig. 1)[28]. Using theoretical pre-

* raphael.lopes@lkb.ens.fr

dictions for the polarizability of the ground state [10, 12] (see also measurements of Ref. [14]), we extract the excited state polarizability, and identify a tensorial component of much larger amplitude than for the ground state. By tuning the relative angle between the laser polarization and an external magnetic field, we find a “magic-polarization” for which the differential light-shift between $|g\rangle$ and $|e\rangle$ is cancelled [20]. As a concrete example of the relevance of this magic-polarization behaviour, we implement a one-dimensional Doppler cooling experiment which we optimize by adjusting the spatially-dependent differential light-shift. We observe a significant gain in phase-space density for the case of a small, positive differential light-shift which leads to an enhanced (red) detuning of the cooling light at the trap center. We interpret this result as a suppression of light-assisted collisions at the bottom of the potential where the atomic density is higher, while cooling remains efficient in the wings.

I. DIFFERENTIAL LIGHT-SHIFT: MAGIC POLARIZATION

The Hamiltonian describing an atom with spin \mathbf{J} in the presence of a constant magnetic field \mathbf{B} and an off-resonant electromagnetic field can be written as

$$\hat{H} = \hat{H}_0 + \hat{H}_{a-l}, \quad (1)$$

$$\text{with } \hat{H}_0 = g_J \mu_B \mathbf{J} \cdot \mathbf{B} \quad \text{and} \quad \hat{H}_{a-l} = \tilde{V}(\mathbf{r}) \mathbf{e}_L^* \underline{\underline{\alpha}} \mathbf{e}_L,$$

where g_J is the Landé g -factor, μ_B the Bohr magneton, \mathbf{e}_L the laser light polarization, and $\tilde{V}(\mathbf{r}) = -\frac{1}{2\epsilon_0 c} I(\mathbf{r})$ where $I(\mathbf{r})$ is the dipole trap laser beam intensity, ϵ_0 the vacuum permittivity and c the speed of light. The dynamic polarizability, $\underline{\underline{\alpha}}$, can be expressed in terms of scalar (α^s), vectorial (α^v) and tensorial (α^t) contributions. In the case of a linearly-polarized laser beam, the vectorial contribution is suppressed and the atom-light interaction can be written as

$$\hat{H}_{a-l} = \tilde{V}(\mathbf{r}) \left\{ \alpha_g^s \mathbb{1} + \alpha_g^t \frac{3(\mathbf{J} \cdot \mathbf{e}_L)^2 - \mathbf{J}^2}{J(2J-1)} \right\}, \quad (2)$$

where α_g^s and α_g^t correspond to the scalar and tensorial components of the polarizability in the ground state manifold.

Assuming that the tensorial contribution to the AC-Stark shift can be treated at first-order in perturbation theory with respect to \hat{H}_0 , the energy shift for the state of lowest energy $|g\rangle$ is given by

$$E_g = E_{g,0} + \tilde{V}(\mathbf{r}) \left\{ \alpha_g^s + \frac{\alpha_g^t}{2} (3 \cos^2 \theta - 1) \right\}, \quad (3)$$

where θ corresponds to the angle between the magnetic field and the orientation of the beam polarization (see Fig. 1). A similar analysis can be performed for the excited electronic level. The energy difference between the states of lowest energy in each manifold, $|g\rangle$ and $|e\rangle$, is then equal to

$$h\nu'_0(\mathbf{r}) = h(\nu_0 + \Delta\nu_\alpha(\mathbf{r})), \quad (4)$$

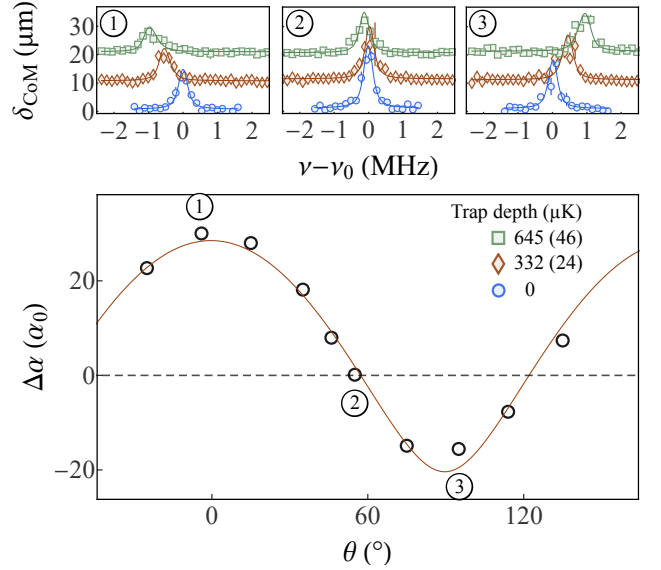


FIG. 2. Differential light-shift as a function of the relative angle θ . Top panels: CoM resonances as a function of the trap depth for the ground state (see legend) for three different angles : 0° , 55° and 100° . The error bars denote the r.m.s. deviation of 3 independent measurements. Main panel: $\Delta\alpha$ as a function of θ . The solid line corresponds to a fit based on the energy difference between excited and ground states following the diagonalization of \hat{H} given in Eq. (1) with $\Delta\alpha^s$ and $\Delta\alpha^t$ as free parameters.

where $h\nu_0 = \Delta E_0 = E_{e,0} - E_{g,0}$, and

$$h\Delta\nu_\alpha(\mathbf{r}) = \tilde{V}(\mathbf{r})\Delta\alpha, \quad (5)$$

where $\Delta\alpha = \Delta\alpha^s + \frac{1}{2}\Delta\alpha^t(3\cos^2\theta - 1)$ and $\Delta\alpha^{(s,t)} = \alpha_e^{(s,t)} - \alpha_g^{(s,t)}$. Importantly, for $|\Delta\alpha^t/\Delta\alpha^s - 1/2| \geq 3/2$, the differential light-shift cancels for a specific polarization angle $\theta_{\text{magic}} = \arccos\left(\sqrt{\frac{1}{3}(1 - 2\frac{\Delta\alpha^s}{\Delta\alpha^t})}\right)$, that we will refer to as a magic-polarization angle in the following text.

We begin by producing a cold sample of 10^7 ^{164}Dy atoms, held in a 1070 nm dipole trap beam. The beam polarization is linear and orientated at approximately 60° relative to the magnetic field (\mathbf{B}_i) initially aligned with the vertical \hat{z} axis (see Fig. 1); as shown hereafter this seemingly arbitrary angle corresponds to θ_{magic} .

In order to probe the resonance frequency for the $|g\rangle \rightarrow |e\rangle$ transition, we apply for $\tau = 30 \mu\text{s}$ a near-resonant beam, circularly polarized (σ^-) and propagating along \hat{z} [29]. The radiation pressure force experienced by the atoms reaches its maximum value when the laser frequency equals the transition frequency. This leads to a maximum displacement of the cloud center-of-mass (CoM) after time-of-flight (ToF), allowing us to extract, as a function of the dipole trap intensity, the transition resonance frequency and the differential light-shift.

In more detail, the mean radiative force exerted on an atom at a position \mathbf{r} is given by [30]

$$\mathbf{F}(\Delta\omega(\mathbf{r}), v_z) = -\hbar k \frac{\Gamma}{2} \frac{s_0}{1 + s_0 + 4 \left(\frac{\Delta\omega(\mathbf{r}) - kv_z}{\Gamma} \right)^2} \hat{\mathbf{z}}, \quad (6)$$

where $k = 2\pi/\lambda$ is the recoil momentum, with $\lambda = 626$ nm, $s_0 = I_0/I_{\text{sat}}$ the saturation parameter with $I_{\text{sat}} = 72 \mu\text{W}/\text{cm}^2$, $\Delta\omega(\mathbf{r}) = 2\pi \times (\nu - \nu'_0(\mathbf{r}))$, v_z is the atomic velocity along $\hat{\mathbf{z}}$, and $\Gamma = 2\pi \times 136$ kHz the transition linewidth. During the application of this red pulse the cloud displacement is negligible (on the order of 1-2 μm) and the pulse therefore solely results in a sudden change of the atomic velocity. Furthermore, the acquired Doppler shift during the pulse is negligible compared to Γ . The optical dipole trap is then immediately switched off and an absorption image is taken after $t_{\text{ToF}} = 1.5$ ms. The momentum kick as a result of the red pulse translates into a CoM position shift, δ_{CoM} , given by

$$\delta_{\text{CoM}} = \frac{t_{\text{ToF}}}{m} \tau \int d\mathbf{v} d\mathbf{r} n(\mathbf{r}, \mathbf{v}) F(\Delta\omega(\mathbf{r}, \mathbf{v})), \quad (7)$$

where $n(\mathbf{r}, \mathbf{v})$ is the normalized spatial and velocity distribution of the cloud, computed for an initial cloud temperature $T \approx 100 \mu\text{K}$ and a harmonic trapping potential with frequencies $\{\omega_x, \omega_{y,z}\} = 2\pi \times \{9(1) \text{ Hz}, 1.9(1) \text{ kHz}\}$.

In Fig. 1 we show a typical CoM-displacement resonance as a function of the laser frequency, ν . The origin of the frequency axis is set by the bare resonance frequency, ν_0 , that we extract from a similar resonance measurement performed in the absence of the trapping beam [31]. Using Eq. (7) we record, for different values of $\tilde{V}(0)$ the resonance position ν'_0 (see Fig. 2 top panels). We verify that ν'_0 varies linearly with $\tilde{V}(0)$ and extract $\Delta\alpha(\theta)$ from the slope. The same procedure is then repeated for several orientations of the magnetic field \mathbf{B}_θ thus probing different relative angles θ (see Fig. 1).

We recover the expected dependence of the total polarizability difference, $\Delta\alpha$, as a function of θ , as shown in Fig. 2 (main panel). We observe that $\Delta\alpha = 0$ for $\theta_{\text{magic}} = 57(2)^\circ$, corresponding to a cancellation of the differential light-shift, and characteristic of magic-polarization behaviour. The fitting function shown in Fig. 2 (main panel) corresponds to the differential light-shift computed numerically from the energy difference between the state of lowest energy ($|g\rangle$) of Eq. (1) and its equivalent solution for the excited state manifold ($|e\rangle$), with free parameters $\Delta\alpha^s$ and $\Delta\alpha^t$. We find $\Delta\alpha^s = -5(2) \alpha_0$ and $\Delta\alpha^t = 33(2) \alpha_0$, where $\alpha_0 = 4\pi\epsilon_0 a_0^3$ and a_0 is the Bohr radius. Using the theoretical values of $\alpha_g^{(s,t)}$ [12] we determine the excited state scalar and tensorial polarizabilities $\alpha_e^s = 179(5) \alpha_0$ and $\alpha_e^t = 35(2) \alpha_0$, respectively. The small error bars reported here are purely statistical but systematic effects beyond the ones that we have probed and discarded can play an important role in the quantitative determination of $\alpha_e^{(s,t)}$. For instance, deviations from the theoretical values of $\alpha_g^{(s,t)}$, such as the ones reported for 1064 nm (see Ref. [14]), would automatically shift the reported absolute values of $\alpha_e^{(s,t)}$. However, the existence of the magic polarization angle (θ_{magic}) is robust with respect to these systematic effects.

Our observations imply that, although the scalar components of the dynamic polarizability are similar for both states, the tensorial contribution of the excited state is much larger than for the ground state. Note however that the tensorial component of the excited state does not alone fulfill the condition $\alpha_e^t > 2\alpha_e^s$ needed to cancel the light-shift of that state.

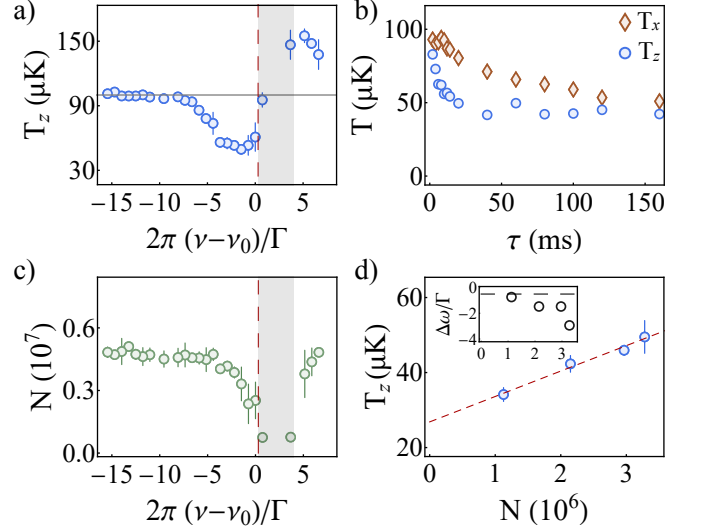


FIG. 3. Doppler cooling efficiency: a) Doppler cooling efficiency for $\theta_{\text{magic}} = 57^\circ$, corresponding to a suppression of the differential light-shift, as a function of the cooling beam frequency ν , for $s_0 = 0.5$ and a pulse time $\tau = 20$ ms. b) T_z and T_x as a function of the cooling beam application time, τ , for $2\pi(\nu - \nu_0) = -\Gamma$. c) Remaining atom number at the end of the $\tau = 20$ ms cooling stage as a function of ν . The vertical dashed line represents the transition resonance. The gray shaded region corresponds to frequencies for which $N < 10^5$. d) Transverse temperature as a function of the initial atom number for $\tau = 20$ ms. The linear fit, red dashed line, allows us to extrapolate a minimal temperature of $27 \mu\text{K}$ for vanishing atom number. Inset: Detuning at which the minimal temperature is recorded as a function of the total atom number. The error bars denote the r.m.s. deviation of 3 independent measurements.

II. APPLICATION TO DOPPLER COOLING

We demonstrate the relevance of a magic-polarization by considering Doppler cooling in an optical dipole trap [32–35]. This process is implemented in order to significantly reduce the cloud temperature over a short timescale, typically set by the weakest trapping frequency. For this purpose we use the 626 nm, narrow line transition considered above where $\Gamma = 2\pi \times 136$ kHz. Since Γ is small compared to the typical differential light-shifts reported in Fig. 2, one expects the cooling efficiency to be strongly dependent on the optical beam polarization.

We use the same optical beam as described in Section I with $\theta = \theta_{\text{magic}}$ [36]. The force experienced by the atoms leads to a mean velocity change in the tightly-confined direction as shown in Fig. 3a. We recover the typical dispersive curve for the kinetic energy as a function of the laser frequency, resulting in cooling (heating) for a red(blue)-detuned frequency. Furthermore, we observe that the energies along the transverse (T_z) and the axial (T_x) axes converge to the same final result over different timescales (see Fig. 3b). The reason for these different dynamics is related to the large trapping potential anisotropy ($\omega_x = 2\pi \times 9(1) \text{ Hz}$, $\omega_z = 2\pi \times 1.9(1) \text{ kHz}$). Indeed, for the relatively small $t_{\text{ToF}} = 1.5$ ms, T_z corresponds to the kinetic energy (momentum distribution), while T_x re-

flects the potential energy along the x -direction (spatial distribution). Although the collisional rate $\Gamma_{\text{coll.}} = 2.5 \times 10^3 \text{ s}^{-1}$ ensures a fast (millisecond timescale) redistribution of the kinetic energy along all three directions, this is not immediately imprinted onto the spatial density distribution; at least a quarter of oscillation period is needed for the cloud size to re-adjust. In our case this corresponds to $\tau > \pi/(2\omega_x) \approx 25 \text{ ms}$ and sets the slow dynamics observed along \hat{x} .

Although the cooling beam detuning is homogeneous over the sample we do not recover the ideal theoretical cooling efficiency. Indeed, the temperature saturates (see Fig. 3b) to $50 \mu\text{K}$, far from the Doppler limit, $T_D \approx 3 \mu\text{K}$. Moreover, a strong enhancement of atom losses occurs at the vicinity of the resonance where cooling efficiency is the highest (see Fig. 3c). Such behaviour suggests that the cloud density is too high for the cooling mechanism to be considered as a single-particle light-matter interaction. A possible explanation is that light-assisted collisions, which are enhanced in the case of large densities, lead to atom losses and heating which counteracts Doppler cooling [12, 37–40].

To study these losses mechanisms in more detail, we investigate the cooling efficiency as a function of the initial atomic density, tuned by varying the atom number before the Doppler cooling stage. As shown in Fig. 3d, we observe a reduction of the temperature as we decrease the atomic density, a signature that the cooling efficiency is indeed bounded by heating processes that are density-dependent. Furthermore, we observe that the detuning at which the minimal temperature is recorded decreases and approaches $-\Gamma/2$, as expected for single-particle Doppler cooling [33]. Both these observations reinforce our assumption that the cooling efficiency is indeed limited by light-assisted collisions. However, we note that even for $N \rightarrow 0$ the temperature does not converge to the Doppler limit $T_D \approx 3 \mu\text{K}$, probably due to technical imperfections of our experimental apparatus.

In order to optimize the cooling efficiency we vary slightly the value of θ around the magic polarization angle θ_{magic} (see Fig. 4). We observe two regimes with distinct behaviour. In the case of a negative differential light-shift ($\Delta\nu_\alpha(\mathbf{r}) < 0$), the cooling is inefficient. On the other hand, for small, positive values of the differential light-shift, we reach lower temperatures than observed for the magic polarization angle. The qualitative explanation for that behaviour is summarized schematically in Fig. 4 (top panels). In the first case, the denser, central, region of the atomic cloud is, due to the strong negative differential light-shift, closer to resonance and therefore interacts strongly with the cooling beam. However the local density is large and light-assisted collisions are predominant; this results in a very low cooling efficiency as shown in Fig. 4a. For the case of a positive differential light-shift the situation is reversed. The central region is strongly detuned, and light-assisted collisions are reduced while cooling taking place in the wings, where the density is lower, is very efficient (see Fig. 4b).

To better understand the above, empirical description of the cooling and heating mechanisms at work, we also report the detuning frequency at which the minimal temperature is recorded for several different values of θ (see Fig. 4c). The

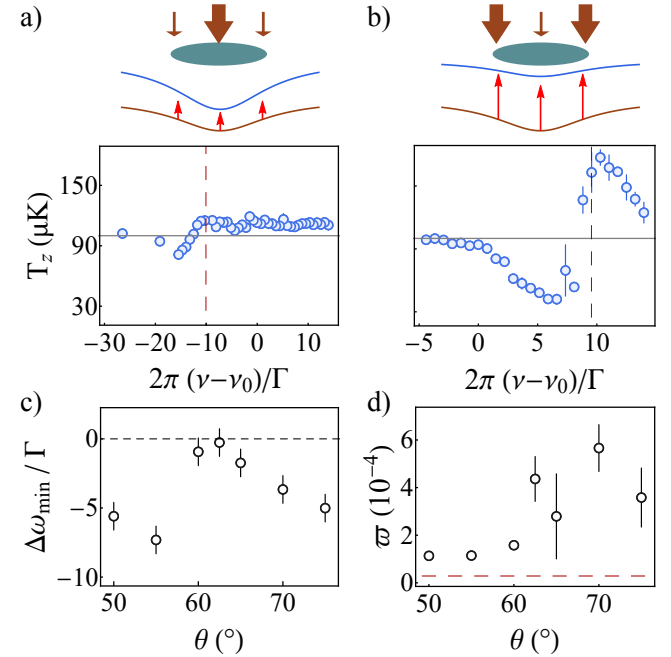


FIG. 4. Doppler cooling efficiency as a function of θ and gain in phase-space density: Cooling efficiency for a) $\theta = 50^\circ$ and b) $\theta = 75^\circ$. The vertical red dashed line indicates the transition resonance at the trap center. c) Detuning from the trap center for which the minimal value of T_z is recorded ($\Delta\omega_{\text{min}}$) as a function of θ . The black dashed line indicates the zero-detuning limit. d) Phase-space density, ϖ , as a function of θ . An optimum is visible for $\theta = 70^\circ$ corresponding to a small, positive differential light-shift. The horizontal dashed red line corresponds to the value of ϖ prior to the Doppler cooling stage. The error bars denote the r.m.s. deviation of 3 independent measurements.

detuning is expressed with respect to the resonance frequency at the trap center, such that $\Delta\omega_{\text{min}} = 2\pi \times (\nu_{\text{min}} - \nu'_0(0))$. In the case of a negative differential light-shift we observe an optimum cooling efficiency for large negative detuning values. This behaviour suggests that the cooling beam is also responsible for local heating and losses at the trap center; processes which are minimized by increasing the absolute frequency detuning. In the case of a differential light-shift cancellation, the detuning is compatible with the textbook $-\Gamma/2$ result. For positive differential light-shifts we also observe an optimum at an enhanced negative detuning. This detuning is expected since the cooling mechanism mainly occurs in the outer regions of the cloud, where the differential light-shift is smaller and therefore the frequency detuning from the trap center is larger (see Fig 4 top panels).

Finally, we optimize the cooling efficiency by maximizing the phase-space density, ϖ , which is a natural figure of merit towards achieving Bose-Einstein condensation. For each value of θ we maximize ϖ by adjusting the detuning frequency and τ . As shown in Fig. 4d, we observe that for small positive differential light-shifts ($\theta \approx 70^\circ$) a maximum is reached, five times larger than the value observed in the case of the magic polarization ($\theta_{\text{magic}} = 57(2)^\circ$). The maximal value of $\varpi = 5.7(10) \times 10^{-4}$ observed for

$\theta = 70^\circ$ corresponds to a gain of approximately 20 compared to the initial phase-space density of the atomic cloud ($\varpi \approx 0.29 \times 10^{-4}$). The maximum phase-space density is reached with small atom losses ($\approx 25\%$), thus setting an interesting starting point for further evaporative cooling.

In conclusion, we have observed the tunability of the differential light-shift for the 626 nm transition in the case of a thermal Dy cloud confined in a far-detuned, 1070 nm, optical dipole trap. We observe that, for a given trapping beam polarization angle, a total cancellation of the differential light-shift

can be achieved. This feature is applied to a Doppler cooling stage in which we observe that a maximum phase-space density is reached in the case of a small, positive differential light-shift. Furthermore, the magic-polarization behaviour opens the prospect of sideband cooling in optical lattices for the purpose of single site imaging [27].

This work is supported by PSL University (MAFAG project) and European Union (ERC UQUAM & TOPODY). We thank Davide Dreon and Leonid Sidorenkov for contributions in earlier stages of the experiment. We also thank Maxence Lepers and Olivier Dulieu for fruitful discussions.

[1] R. M. Wilson, S. Ronen, J. L. Bohn, and H. Pu, *Phys. Rev. Lett.* **100**, 245302 (2008).

[2] L. Santos, G. V. Shlyapnikov, and M. Lewenstein, *Phys. Rev. Lett.* **90**, 250403 (2003).

[3] A. Boudjemâa and G. V. Shlyapnikov, *Phys. Rev. A* **87**, 025601 (2013).

[4] L. Chomaz, R. M. W. van Bijnen, D. Petter, G. Faraoni, S. Baier, J. H. Becher, M. J. Mark, F. Wächtler, L. Santos, and F. Ferlaino, *Nature Physics* (2018), 10.1038/s41567-018-0054-7.

[5] S. Nascimbène, *Journal of Physics B: Atomic, Molecular and Optical Physics* **46**, 134005 (2013).

[6] X. Cui, B. Lian, T.-L. Ho, B. L. Lev, and H. Zhai, *Phys. Rev. A* **88**, 011601 (2013).

[7] N. Q. Burdick, Y. Tang, and B. L. Lev, *Phys. Rev. X* **6**, 031022 (2016).

[8] I. Ferrier-Barbut, H. Kadau, M. Schmitt, M. Wenzel, and T. Pfau, *Phys. Rev. Lett.* **116**, 215301 (2016).

[9] H. Kadau, M. Schmitt, M. Wenzel, C. Wink, T. Maier, I. Ferrier-Barbut, and T. Pfau, *Nature* **530**, 194 EP (2016).

[10] V. A. Dzuba, V. V. Flambaum, and B. L. Lev, *Phys. Rev. A* **83**, 032502 (2011).

[11] H. Li, J.-F. m. c. Wyart, O. Dulieu, and M. Lepers, *Phys. Rev. A* **95**, 062508 (2017).

[12] H. Li, J.-F. Wyart, O. Dulieu, S. Nascimbène, and M. Lepers, *Journal of Physics B: Atomic, Molecular and Optical Physics* **50**, 014005 (2017).

[13] W. Kao, Y. Tang, N. Q. Burdick, and B. L. Lev, *Opt. Express* **25**, 3411 (2017).

[14] C. Ravensbergen, V. Corre, E. Soave, M. Kreyer, S. Tzanova, E. Kirilov, and R. Grimm, *ArXiv e-prints* (2018), arXiv:1801.05658 [physics.atom-ph].

[15] J. H. Becher, S. Baier, K. Aikawa, M. Lepers, J.-F. Wyart, O. Dulieu, and F. Ferlaino, *Phys. Rev. A* **97**, 012509 (2018).

[16] T. Maier, H. Kadau, M. Schmitt, A. Griesmaier, and T. Pfau, *Opt. Lett.* **39**, 3138 (2014).

[17] E. Lucioni, G. Masella, A. Fregosi, C. Gabbanini, S. Gozzini, A. Fioretti, L. Del Bino, J. Catani, G. Modugno, and M. Inguscio, *The European Physical Journal Special Topics* **226**, 2775 (2017).

[18] E. Lucioni, L. Tanzi, A. Fregosi, J. Catani, S. Gozzini, M. Inguscio, A. Fioretti, C. Gabbanini, and G. Modugno, *ArXiv e-prints* (2018), arXiv:1803.10676 [cond-mat.quant-gas].

[19] N. Lundblad, M. Schlosser, and J. V. Porto, *Phys. Rev. A* **81**, 031611 (2010).

[20] H. Kim, H. S. Han, and D. Cho, *Phys. Rev. Lett.* **111**, 243004 (2013).

[21] S. Stellmer, B. Pasquiou, R. Grimm, and F. Schreck, *Phys. Rev. Lett.* **110**, 263003 (2013).

[22] M. Takamoto, F.-L. Hong, R. Higashi, and H. Katori, *Nature* **435**, 321 EP (2005).

[23] R. Le Targat, X. Baillard, M. Fouché, A. Brusch, O. Tcherbakoff, G. D. Rovera, and P. Lemonde, *Phys. Rev. Lett.* **97**, 130801 (2006).

[24] Z. W. Barber, J. E. Stalnaker, N. D. Lemke, N. Poli, C. W. Oates, T. M. Fortier, S. A. Diddams, L. Hollberg, C. W. Hoyt, A. V. Taichenachev, and V. I. Yudin, *Phys. Rev. Lett.* **100**, 103002 (2008).

[25] H. Katori, K. Hashiguchi, E. Y. Il'inova, and V. D. Ovsiannikov, *Phys. Rev. Lett.* **103**, 153004 (2009).

[26] B. J. Bloom, T. L. Nicholson, J. R. Williams, S. L. Campbell, M. Bishop, X. Zhang, W. Zhang, S. L. Bromley, and J. Ye, *Nature* **506**, 71 EP (2014).

[27] H. Ott, *Reports on Progress in Physics* **79**, 054401 (2016).

[28] The 1070 nm laser light is provided by a commercial multi-mode IPG (50W) laser. A similar magic-polarization behaviour was observed using a 1064 nm single-mode Azur Light (40W) laser.

[29] We use a collimated beam with a waist of 5.5 mm, much wider than the cloud spatial extension and therefore uniform for the sample. We have also performed several experiments with different pulse durations but did not observe significant changes of the differential light-shift as a function of the pulse length. The 30 μ s pulse length thus corresponds to the shortest pulse guaranteeing a good SNR.

[30] C. Foot, *Atomic physics*, Oxford master series in physics (Oxford University Press, 2005).

[31] We checked that nor the red-pulse duration length ($10 < \tau < 100 \mu$ s) nor the cloud temperature affected substantially the value of ν_0 .

[32] P. D. Lett, W. D. Phillips, S. L. Rolston, C. E. Tanner, R. N. Watts, and C. I. Westbrook, *J. Opt. Soc. Am. B* **6**, 2084 (1989).

[33] J. Dalibard and C. Cohen-Tannoudji, *J. Opt. Soc. Am. B* **6**, 2023 (1989).

[34] P. O. Schmidt, S. Hensler, J. Werner, T. Binhammer, A. Görlitz, and T. Pfau, *J. Opt. Soc. Am. B* **20**, 960 (2003).

[35] T. Maier, *Interactions in a Quantum Gas of Dysprosium Atoms*, Ph.D. thesis, Universität Stuttgart (2015).

[36] A 2 G bias field ensures that the Zeeman splitting is much larger than the transition linewidth. Therefore, small imperfections of the laser beam polarization are not particularly relevant. Furthermore, the weak Clebsch-Gordan coefficients for π and σ^+ transitions compared to the σ^- transition render these imperfections even less relevant.

[37] A. Gallagher and D. E. Pritchard, *Phys. Rev. Lett.* **63**, 957 (1989).

- [38] P. S. Julienne and J. Vigu , Phys. Rev. A **44**, 4464 (1991).
- [39] J. Weiner, V. S. Bagnato, S. Zilio, and P. S. Julienne, Rev. Mod. Phys. **71**, 1 (1999).
- [40] D. Dreon, L. A. Sidorenkov, C. Bouazza, W. Maineult, J. Dalibard, and S. Nascimbene, Journal of Physics B: Atomic, Molecular and Optical Physics **50**, 065005 (2017).